

## State of Charge (SOC) Estimation of Lithium-ion Battery Based on Adaptive Square Root Unscented Kalman Filter

Wang Kai<sup>1,\*</sup>, Feng Xiao<sup>1</sup>, Pang Jinbo<sup>2</sup>, Ren Jun<sup>1</sup>, Duan Chongxiong<sup>3</sup>, Li Liwei<sup>1,\*</sup>

<sup>1</sup> School of Electrical Engineering, Qingdao University, Qingdao, 266071, China

<sup>2</sup> Collaborative Innovation Center of Technology and Equipment for Biological Diagnosis and Therapy in Universities of Shandong, Institute for Advanced Interdisciplinary Research (iAIR), University of Jinan, Shandong, Jinan 250022, China

<sup>3</sup> School of Materials Science and Energy Engineering, Foshan University, Foshan, 528231, China

\*E-mail: [wkwj888@163.com](mailto:wkwj888@163.com) and [ytlw@163.com](mailto:ytlw@163.com)

Received: 8 May 2020 / Accepted: 19 July 2020 / Published: 10 August 2020

---

The improved battery management system (BMS) can give full play to the best performance of power battery, and the state of charge (SOC) estimation of power lithium-ion battery is the core and key technology of BMS. The Kalman filter method with the first-order Thevenin model cannot obtain better estimation results because of the limited model precision. Aiming at solving the above problems, this paper presents a second-order Thevenin equivalent circuit model. The idea of the Sage-Husa adaptive algorithm and square root filter is introduced based on the Unscented Kalman Filter (UKF) algorithm. The adaptive square root Unscented Kalman Filter (ASRUKF) algorithm is formed to improve the precision of SOC estimation. Experiments on SOC estimation of the battery are carried out under three different working conditions. The experimental results show that the ASRUKF algorithm under the second-order Thevenin equivalent circuit model can converge quickly and achieve high precision in SOC estimation.

---

**Keywords:** lithium-ion battery, SOC estimation, equivalent circuit model, adaptive square root Unscented Kalman Filter

### 1. INTRODUCTION

With facing the massive demand for fossil fuels and severe pollution to the ecological environment, electric vehicles have gradually entered people's field of vision with their advantages of energy saving and environmental protection, which have become a new industry of great concern. The power lithium battery plays a significant role as the energy source of electric vehicles. The performance of BMS determines the endurance kilometers, the performance, and the promotion degree of the electric

vehicles directly. Moreover, SOC is the core and critical technical difficulty of BMS. It provides the use state of battery for the whole BMS system, and it is the basis for realizing the functions of other battery management [1-3]. The SOC is also known as the battery's remaining charge, which represents the ratio of the battery's remaining available charge at a given moment to its rated capacity. Accurate SOC estimation has always been a rigid demand of BMS. However, the SOC of the batteries cannot be measured directly because of its particularity; it needs to be estimated by the external characteristics of the batteries [4-7]. Furthermore, its estimation precision is influenced by many factors, such as model, algorithm, working condition, error, and SOC estimation, so SOC estimation has always been the key and difficult point in the field of the research of battery technology.

At present, the standard methods of SOC estimation are open-circuit voltage method, discharge experiment method, Ann-hour integral method, linear model method, internal resistance method, Kalman filter algorithm, neural network algorithm, and fuzzy logic algorithm [8-14]. Although the open-circuit voltage method can obtain a more accurate SOC value, it cannot realize the on-line test of SOC. The stable open-circuit voltage can only be obtained after the battery is left standing for several hours, which is not suitable for the measurement of the system in operation [9, 10]. The discharge experiment method requires a significant amount of time to remove the battery from the system, so it is also not suitable for estimating the SOC under the working state [11-13]. The ampere-hour integral method will have errors in the process of measurement; the precision of the estimation depends on the precision of the initial given SOC reference value. Therefore, long-term use will lead to a continuous increase of all kinds of error accumulation, resulting in a significant estimation deviation [15-18]. The linear model method is simple and has a narrow range of applications, so it cannot accurately reflect the state change of the SOC estimation of the strongly nonlinear system. Although the internal resistance value is related to SOC estimation, the characteristics of internal resistance are not clear, the applicable battery types are not universal, and the measurement is difficult, which is not suitable for the current technical level [19-24]. The neural network algorithm needs a large number of accurate and comprehensive battery sample data to train, which is not only a huge workload, but also requires a large amount of time. Besides, the precision of the estimation results is greatly affected by the training data and training methods, so it is not suitable for the system that requires high precision and stability [25-27]. The establishment of fuzzy rules in the fuzzy logic algorithm is not systematic and scientific, and the quality of control precision cannot be guaranteed completely. The problems of stability and robustness also need to be solved [28-30].

Kalman filter algorithm is an optimal autoregressive data filtering algorithm, which can estimate the optimal state of complex dynamic systems according to the principle of minimum mean-variance [31-33]. It can not only correct the initial error of the system and correct the system in operation, but also effectively suppress the noise in the actual measurement process. Therefore, it is one of the ideal self-correcting SOC estimation methods. However, this method has a strong dependence on the precision of the battery model, and it is susceptible to the dynamic parameters of the battery, which is the primary method used in this paper.

## 2. THE PROPOSAL OF EQUIVALENT CIRCUIT MODEL

The estimation of SOC by Kalman filter algorithm depends on the accurate battery model, so selecting the appropriate model is crucial to the state estimation of the battery. The equivalent circuit model is a circuit network based on the series-parallel form of essential circuit components, such as resistance, capacitance, and voltage source [34-38]. Analogous to the battery, it can simulate the characteristics such as internal ohmic resistance and polarization reaction. And its circuit structure is intuitive and concise, simple and clear, easy to establish the state space equation of estimating variables, which is convenient for battery simulation analysis and parameter identification [39-42]. Therefore, this kind of model is widely used in the SOC estimation of batteries [12, 13]. Common equivalent circuit models include the Rint model, Thevenin model, PNGV model, and GNL-model.

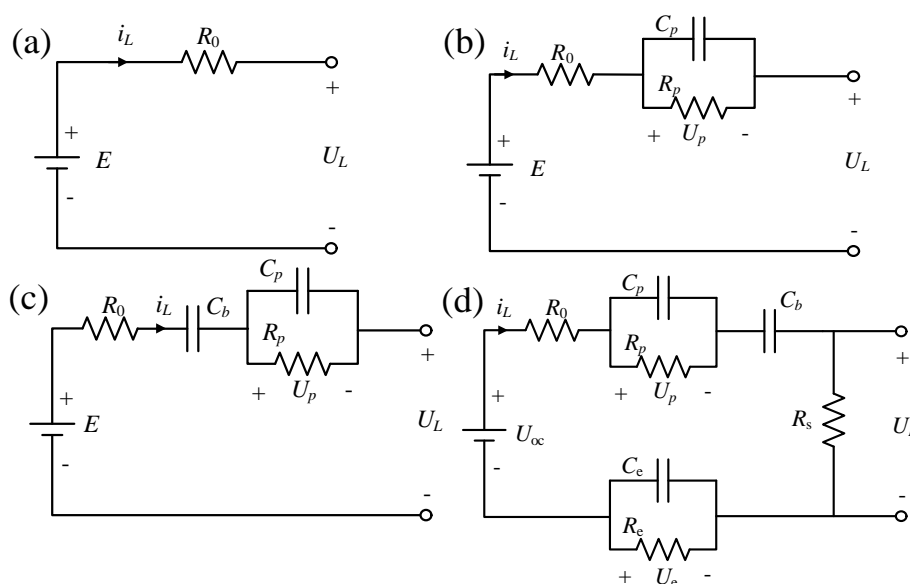


**Figure 1.** The equivalent models of Li-ion battery (a) Rint model (b) Thevenin model (c) PNGV model (d) GNL-model

The equivalent circuit of Rint model is shown in Figure 1(a). The model is extremely simple and it consists of an ideal voltage source  $E$  in series with a simple internal resistance  $R_0$ . However, due to its poor accuracy, it cannot represent the influence of electrochemical reaction inside the cell. And it belongs to a linear model, which is not suitable for SOC estimation in practical application [43, 44]. The equivalent circuit of Thevenin model is shown in Figure 1(b). On the basis of Rint model, a parallel RC branch is added to the Thevenin equivalent circuit model to simulate the polarization effect in the charging and discharging process of Li-ion batteries. To a certain extent, it can reflect the dynamic characteristics of Li-ion battery, which makes up for the limitations and shortcomings of Rint model. However, due to the complexity of the actual battery operation, the dynamic performance of a single RC branch is limited, which cannot accurately reflect the polarization effect or other influencing factors of the battery [45-47]. PNGV model (Figure 1(c)) adds a plate capacitance  $C_b$  on the basis of Thevenin equivalent circuit model, which is used to simulate the characteristics of battery OCV changing with the accumulation of current, so its accuracy is higher than that of the Thevenin model. However, this model is difficult to identify

parameters and has high complexity in calculation, so it is not suitable for real-time SOC estimation in practical application [48-50]. The equivalent circuit of GNL-model is shown in Figure 1(d). This model is the induction and development of the Rint model, Thevenin model and PNGV model, which combines the characteristics of all models. However, there are many resistance and capacitance components inside the model, the dynamic order is too high, and the parameter data need to be processed is too much, so it is difficult to identify and calculate, which is not suitable for real-time SOC estimation in engineering applications [51-53].

Comprehensive comparative analysis of the advantages and disadvantages of the several above models, this paper uses the Thevenin equivalent model. Compared with other models, the Thevenin model can better reflect the dynamic characteristics of the battery [54-57]. In this paper, the Thevenin equivalent circuit model with the second-order RC branch is selected. The second-order RC model can more accurately reflect the dynamic characteristics of the battery than the first-order Thevenin model, thus significantly improving the precision of the equivalent circuit model. Although the precision of the second-order RC model is slightly lower than that of the third-order and fourth-order models, when the RC branch exceeds the second-order, the calculation and complexity are significantly increased when the model precision is not improved significantly [58-61]. Considering the precision of the model, the degree of complexity, and the amount of calculation, the Thevenin equivalent circuit model of the second-order RC branch is more suitable for the performance simulation of Li-ion batteries in this paper.

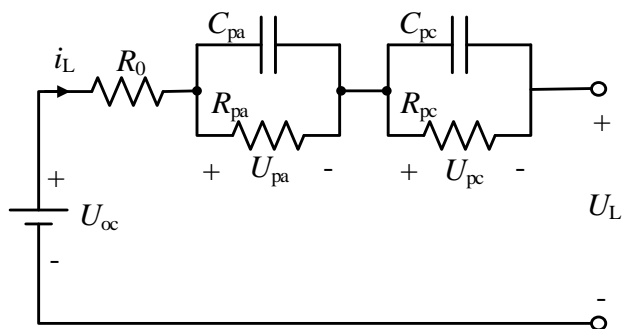


**Figure 2.** The equivalent circuit model based on 2RC-Thevenin model of Li-ion battery

In Figure 2,  $U_{oc}$  denotes the open-circuit voltage (OCV),  $U_L$  denotes the external voltage of the battery, and  $i_L$  denotes the output current of the battery.  $R_0$  is the equivalent ohmic resistance of the cell,  $R_{pa}$  and  $R_{pc}$  represent the equivalent internal resistance generated by the electrochemical polarization and concentration polarization of the cell, respectively. The  $R_{pa}$  and  $C_{pa}$  are equivalent to the impedance received upon transport between Li-ion electrodes. The time constant  $\tau_1$  is small, and the  $U_{pa}$  is the voltage value at both ends of  $R_{pa}$  and  $C_{pa}$ .  $R_{pc}$  and  $C_{pc}$  are equivalent to the impedance of lithium ions upon diffusion in the electrode material. The time constant  $\tau_2$  is large, and  $U_{pc}$  is the voltage value at both ends of  $R_{pc}$  and  $C_{pc}$ . The following mathematical relations can be obtained from the Thevenin theorem:

$$U_{oc} = i_L R_0 + U_{pa} + U_{pc} + U_L \tag{1}$$

$$i_L = \frac{U_{pa}}{R_{pa}} + C_{pa} \frac{dU_{pa}}{dt} \tag{2}$$

$$i_L = \frac{U_{pc}}{R_{pc}} + C_{pc} \frac{dU_{pc}}{dt} \tag{3}$$

From the above formulas (1), (2), (3), we can deduce the relationship between the voltage at both ends of  $C_{pa}$  and  $C_{pc}$  and its derivative and the output current  $i_L$ . And the following equation of state can be established:

$$\begin{bmatrix} \dot{U}_{pa} \\ \dot{U}_{pc} \end{bmatrix} = \begin{bmatrix} -\frac{1}{R_{pa}C_{pa}} & 0 \\ 0 & -\frac{1}{R_{pc}C_{pc}} \end{bmatrix} \cdot \begin{bmatrix} U_{pa} \\ U_{pc} \end{bmatrix} + \begin{bmatrix} \frac{1}{C_{pa}} \\ \frac{1}{C_{pc}} \end{bmatrix} \cdot i_L \tag{4}$$

The functional relationship of OCV-SOC is strongly nonlinear, and pulse discharge experiments can obtain the relationship between them. The battery adopts the standard 18650 lithium battery, and the battery is discharged at full charge with 1C current. When the SOC drops by 5%, it will stand for 10 minutes. The test curve of pulse discharge is shown in Figure 3.

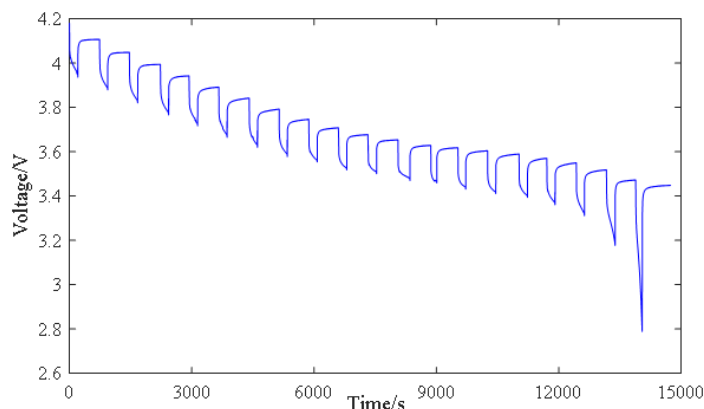


**Figure 3.** The testing curve of pulse discharge

The SOC value of the battery at each moment can be calculated by the ratio of the battery discharge recorded in the electronic load to the rated battery. The OCV values of all the measuring points at each interval of about 5% can be obtained by the upper computer of the electronic load and the Dspace MicroLab Box.

The OCV-SOC relationship curve between  $U_{oc}$  and SOC measured experimentally is shown in Figure 4. And the function expression of the OCV-SOC relationship curve can be obtained by fitting the polynomial of the least square method at 5% test data points from 0 to 1:

$$U_{oc} = F(SOC) = 11.65 * SOC^7 - 35.01 * SOC^6 + 40.4 * SOC^5 - 24.87 * SOC^4 + 11.73 * SOC^3 - 4.439 * SOC^2 + 1.28 * SOC + 3.42 \tag{5}$$

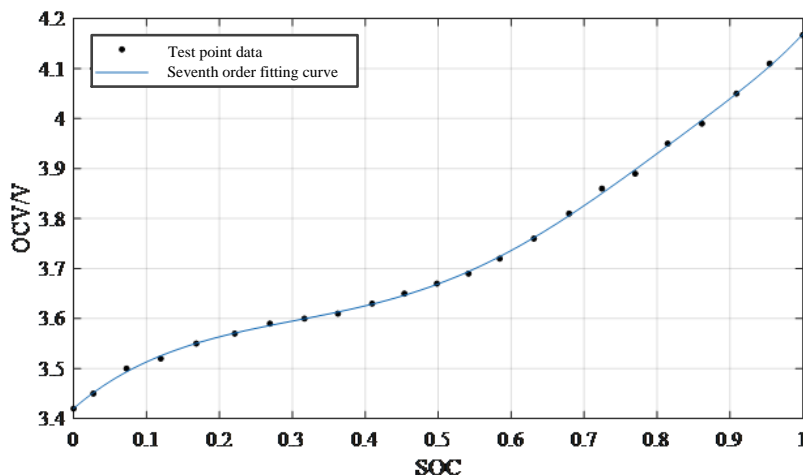


Figure 4. OCV vs. SOC relationship curve

The functional relationship of SOC of the battery can be obtained by the improved Ann-hour integral method:

$$SOC_{(t)} = SOC_{(t_0)} + \frac{1}{\beta_T Q_N} \int_{t_0}^t \eta_i i_L dt \tag{6}$$

In formula (6),  $i_L$  is the charge/discharge current at the current moment, and  $\eta_i$  represents the current correction coefficient at different charge/discharge rates,  $Q_N$  is the rated capacity of the cell, and  $\beta_T$  is the correction coefficient of the actual capacity of the cell at the thermodynamic temperature T.

The discrete model of lithium-ion batteries can be described as follows:

$$\begin{aligned} x_{k+1} &= F(x_k, u_k) + w_k \\ y_k &= H(x_k, u_k) + v_k \\ w_k &\sim (0, Q_k) \\ v_k &\sim (0, R_k) \end{aligned} \tag{7}$$

In Formula (7),  $x_k$ ,  $x_{k+1}$  is the status of the system;  $y_k$  is the observed quantity;  $u_k$  is the controlled quantity;  $w_k$  is white Gaussian noise generated by the system, with the mean value of 0, and the covariance of  $Q_k$ . And  $v_k$  is the white Gaussian noise that is not related to  $w_k$  generated in the observation process, with a mean value of 0 and a covariance of  $V_k$ . Combined with the equivalent circuit model established in Figure 2, each variable is defined as follows:

$$\begin{aligned} x &= [SOC \quad U_{pa} \quad U_{pc}]^T \\ u &= i_L \\ y &= U_L \end{aligned} \tag{8}$$

Formula F1, F2 and F3 are obtained according to equations (6), (2) and (3), and observation equation (11) is obtained by discretization according to equation (1).

$$x_{k+1} = F(x_k, u_k) = [F_1 \quad F_2 \quad F_3]_k^T \tag{9}$$

$$\begin{cases} F_1 = x_1 - \frac{\eta_i \Delta t}{\beta_T Q_N} u & (10) \\ F_2 = \exp(-\frac{\Delta t}{R_{pa} C_{pa}}) x_2 + (1 - \exp(-\frac{\Delta t}{R_{pa} C_{pa}})) u \\ F_3 = \exp(-\frac{\Delta t}{R_{pc} C_{pc}}) x_3 + (1 - \exp(-\frac{\Delta t}{R_{pc} C_{pc}})) u \\ y_k = H(x_k, u_k) = U_{oc}(x_{1,k}) - x_{2,k} - x_{3,k} - u_k R_0 & (11) \end{cases}$$

### 3. IDENTIFICATION OF MODEL PARAMETERS

There are five components in the second-order Thevenin equivalent circuit model, which need to be parameter identification, namely ohmic internal resistance  $R_0$ , polarization resistance  $R_{pa}$ ,  $R_{pc}$  and polarization capacitance  $C_{pa}$ ,  $C_{pc}$ . Similarly, the identification is carried out under the pulse discharge experiment, and the pulse discharge curve at SOC=95% is intercepted in Figure 3 to illustrate. Figure 5 shows the pulse discharge voltage curve when SOC=95%.

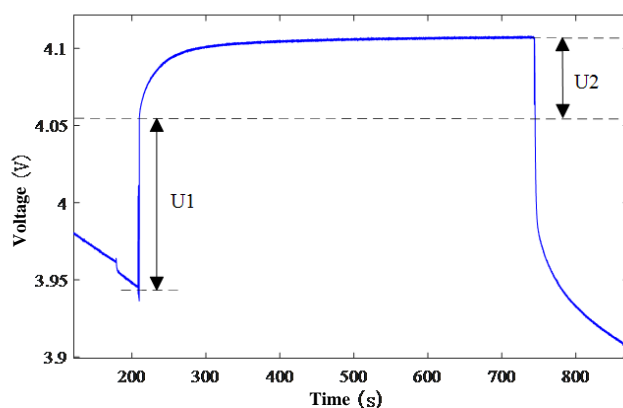


**Figure 5.** Terminal voltage curve when SOC=95%

In Figure 5, when the current is equal to 1C, the pulse discharge process is from 0s to about 210s. When the pulse discharge stops at about 210s, and the voltage changes  $U_1$  instantly, which is caused by the ohmic internal resistance  $R_0$  inside the battery. According to ohm's law, the  $R_0$  value of this point can be obtained from the formula  $R_0 = U_1 / i_L$ . The slowly varying voltage between about 210s and 740s is caused by two sets of RC branches in parallel in the equivalent circuit. The change in voltage is  $U_2$ . In this process of slow change, the output equation of terminal voltage is expressed as:

$$U = U_{oc} + R_0 i_L + R_{pa} i_L (1 - e^{-t/\tau_1}) + R_{pc} i_L (1 - e^{-t/\tau_2}) \quad (12)$$

Where  $\tau_1$ ,  $\tau_2$  are time constant,  $\tau_1 = R_{pa} C_{pa}$ ,  $\tau_2 = R_{pc} C_{pc}$ , and  $\tau_1 < \tau_2$ . The four-parameter values of SOC corresponding to  $R_{pa}$ ,  $C_{pa}$ ,  $R_{pc}$  and  $C_{pc}$  can be fitted by an exponential function. The function formula selected is as follows:

$$U=k_0+k_1e^{-t/\tau_1}+k_2e^{-t/\tau_2} \tag{13}$$

With the slowly changing terminal voltage curve data of the U2 segment in Figure 5, the least square method is used for parameter fitting identification in the MATLAB environment. In this way, we can obtain the parameters  $k_0$ 、 $k_1$ 、 $k_2$ 、 $\tau_1$  and  $\tau_2$  in the formula, and get the voltage curves as shown in Figure 6.

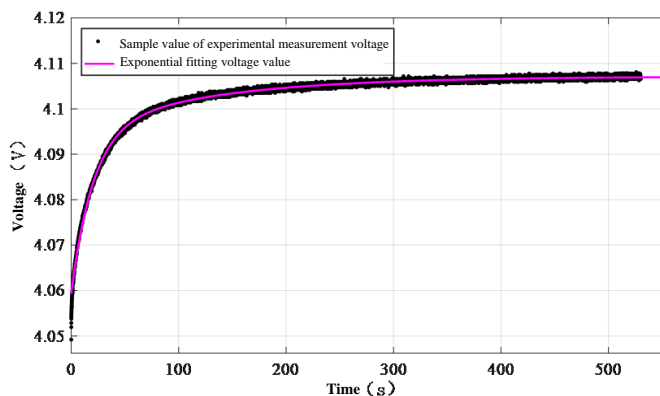


**Figure 6.** Parameter identification fitting curve when SOC=95%

In formula (13), the  $k_0$  corresponds to the open-circuit voltage after the voltage of the curve is stable,  $k_1$  corresponds to the  $-R_{paiL}$  in formula (12),  $k_2$  corresponds to the  $-R_{pciL}$  in formula (11),  $\tau_1$  and  $\tau_2$  correspond to the time constant  $\tau_1$  and  $\tau_2$  in formula (12). The corresponding values of  $R_{pa}$ ,  $C_{pa}$ ,  $R_{pc}$  and  $C_{pc}$  are as follows:

$$R_{pa} = -\frac{k_1}{i_L} \quad R_{pc} = -\frac{k_2}{i_L} \quad C_{pa} = \frac{\tau_1}{R_{pa}} \quad C_{pc} = \frac{\tau_2}{R_{pc}} \tag{14}$$

In the same way as establishing the OCV-SOC curve relationship, the functional relationship of SOC values corresponding to  $R_0$ ,  $R_{pa}$ ,  $C_{pa}$ ,  $R_{pc}$  and  $C_{pc}$  is determined by interpolation fitting, and the dynamic curves of each parameter about SOC are obtained.

To verify the performance of the established Li-ion battery equivalent circuit model, and the precision of parameter identification, the equivalent circuit model of Li-ion battery was established in Simulink simulation environment in MATLAB. The Simulink simulation model established according to the results of parameter identification, and the specific parameters of the lithium-ion battery are shown in Figure 7.

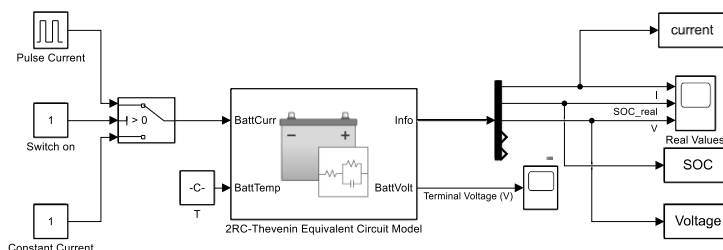


**Figure 7.** The 2RC battery simulation model

#### 4. ADAPTIVE SQUARE ROOT UNSCENTED KALMAN FILTER

In the SOC estimation of the battery, the Kalman filter algorithm has a high requirement for the precision of the battery model. However, in the actual operation of the battery, the precision of the model will be reduced due to the changes in the ambient temperature and parameters. At the same time, in the actual working environment, the measurement of the characteristics of the battery also has the interference of strong random noise, and the inevitable measurement error [62-73]. These problems will affect the precision and stability of SOC estimation results. In order to solve the above problems, the idea of an adaptive filter is introduced based on the unscented Kalman filter to form an adaptive unscented Kalman filter (AUKF). The adaptive filter is based on the UT transform. The Sage-Husa adaptive algorithm is used to optimize the mean and covariance of the process noise  $w_k$  and observation noise  $v_k$  to reduce the deviation caused by the uncertainty noise to the system estimation results, which can effectively prevent the algorithm from diverging and make the estimated variable restore the true value to the maximum extent [74-78].

However, when the adaptive algorithm was added to the MATLAB simulation of SOC estimation, the problem of negative determination of covariance appeared, resulting in an imaginary number of variables in the program and leading to the failure of the program [79-83]. To solve this problem, the idea of Square Root (SR) filter was introduced, which was fused into the AUKF algorithm to form ASRUKF.

The square root filtering algorithm used in this paper is fused to the AUKF algorithm. Its steps mainly include four parts: initialization, sigma point calculation, time update, and measurement update [84-88].

Step 1: Initialize the state vector  $x$ . Covariance  $P_0$  is obtained from the initial value  $x_0$ . The square root initial value  $S_0$  is obtained from  $P_0$ . Using covariance square root  $S_k$  instead of  $P_k$  in UT transform and UKF algorithm steps to participate in recursive computation:

$$\begin{cases} x_0 = E(x_0) \\ S_0 = chol\{P_0\} = chol\{[(x_0 - x_0)(x_0 - x_0)^T]\} \end{cases} \quad (15)$$

Step 2: Using the UT transform to calculate Sigma point:

$$\chi_k = [x_k \quad x_k + \eta S_k \quad x_k - \eta S_k] \quad (16)$$

Step 3: Time update. Including state estimate  $\chi_{k+1|k}$  of each Sigma point, output estimate  $y_{k+1|k}$ , state estimates  $x_{k+1|k}$  for weighted  $k+1$  moments, output estimate  $y_{k+1}^-$ , and the square root of covariance  $S_{k+1}^-$ :

$$\chi_{k+1|k} = f[\chi_k, u_k] \quad (17)$$

$$\bar{x}_{k+1} = \sum_{i=0}^{2n} \omega_m^{(i)} \chi_{k+1|k} \quad (18)$$

$$S_{k+1}^- = qr\{[\sqrt{\omega_c^{-1}}(\chi_{1:2n,k+1|k} - \bar{x}_{k+1})\sqrt{Q_{k+1}}]\} \quad (19)$$

$$S_{k+1}^- = cholupdate\{S_{k+1}^-, \chi_{0,k+1|k} - \bar{x}_{k+1}, \omega_c^0\} \quad (20)$$

$$y_{k+1|k} = h[\chi_{k+1|k}] \quad (21)$$

$$y_{k+1}^- = \sum_{i=0}^{2n} \omega_m^i y_{i,k+1|k} \quad (22)$$

In the process of recursion, since  $\omega_c^0$  maybe negative, formula (20) needs to be added after formula (19) to ensure the non-negative nature of the matrix, so that:

$$S_{k+1}^- = S_{k+1}^- \pm \sqrt{|\omega_c^0|} (\chi_{0,k|k-1} - \hat{x}_{k+1}^-)(\chi_{0,k|k-1} - \hat{x}_{k+1}^-)^T \tag{23}$$

Step 4: Measurement update. Including the covariance square root  $S_{y_{k+1}}$  of the output residual, the mutual covariance  $P_{x_{k+1}y_{k+1}}$  of the state estimate and the output estimate:

$$S_{y_{k+1}} = qr\{[\sqrt{\omega_c^0} (y_{1:2n,k+1|k} - y_{k+1}^-) \quad \sqrt{R_{k+1}}]\} \tag{24}$$

$$S_{y_{k+1}} = cholupdate\{S_{y_{k+1}}, y_{0,k+1|k} - y_{k+1}^-, \omega_c^0\} \tag{25}$$

$$P_{x_{k+1}y_{k+1}} = \sum_{i=0}^{2n} \omega_c^i [\chi_{i,k+1|k} - x_{k+1}^-][y_{i,k+1|k} - y_{k+1}^-] \tag{26}$$

And the update of the Kalman gain matrix  $K_{k+1}$  of the system, the posterior estimate  $x_{k+1}$  of the state variable  $x$  and the square root  $S_{k+1}$  of the state estimation error co-defense:

$$K_{k+1} = (P_{x_{k+1}y_{k+1}} / S_{y_{k+1}}^T) / S_{y_{k+1}} \tag{27}$$

$$x_{k+1} = x_{k+1}^- + K_{k+1} (y_{k+1} - y_{k+1}^-) \tag{28}$$

$$U = K_{k+1} S_{y_{k+1}} \tag{29}$$

$$S_{k+1} = cholupdate\{S_{k+1}^-, U, -1\} \tag{30}$$

The idea of an adaptive algorithm and square root filter is incorporated based on the UKF algorithm. The formed ASRUKF algorithm can not only improve the numerical instability of UKF algorithm, but also correct the error caused by the time-varying noise. Based on obtaining stable results, it can obtain higher precision than UKF algorithm.

### 5. INTERPRETATION OF RESULT

The experimental object selected in this paper is the universal 18650 model dynamic lithium-ion battery, whose rated capacity is 2.2Ah, rated voltage is 3.7V, charging cut-off voltage is 4.2V, charging cut-off current is 0.01A, discharging cut-off voltage is 2.75V. The experimental temperature is controlled at 20°C. The test platform of the 18650-powered lithium-ion battery consists of a DC stabilized power supply, a DC electronic load, a Dspace MicroLab Box, and a computer. The state of battery charging and discharging is controlled by DC power supply and electronic load. The Dspace MicroLab Box can realize the high precision measurement of the characteristics of the battery and the high-speed operation of the program, and display the real-time experimental data of various state quantities and variables through the Control Desk of the upper computer software on the computer terminal [89-95].

First of all, the model parameters were identified, and the pulse discharge experiment was carried out. The test point is 5% of the SOC interval. After the parameter identification of the least square method, the experimental platform of pulse discharge is shown in Figure 8 below:

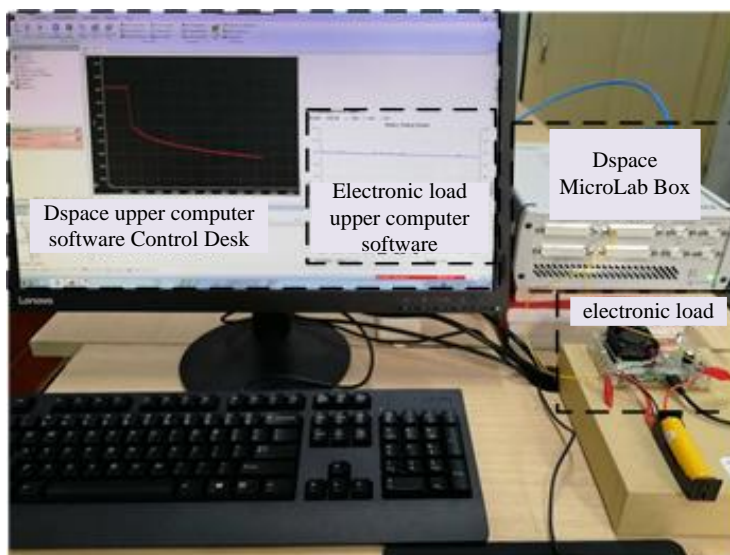


Figure 8. Experimental platform of pulse discharge

After the parameter identification is completed, the SOC estimation experiment of a lithium-ion battery is carried out. Firstly, the simulation analysis was carried out under the constant discharge mode. For the convergence of the ASRUKF algorithm, the different initial values were given for the simulation analysis, as shown in Figure 9. In this simulation, the true value at the initial moment of SOC is selected as 95%, while the estimated initial values of the algorithm are selected as 100%, 80%, 65% and 50%, corresponding to the initial errors are +5%, -15%, -30% and -45%, respectively.

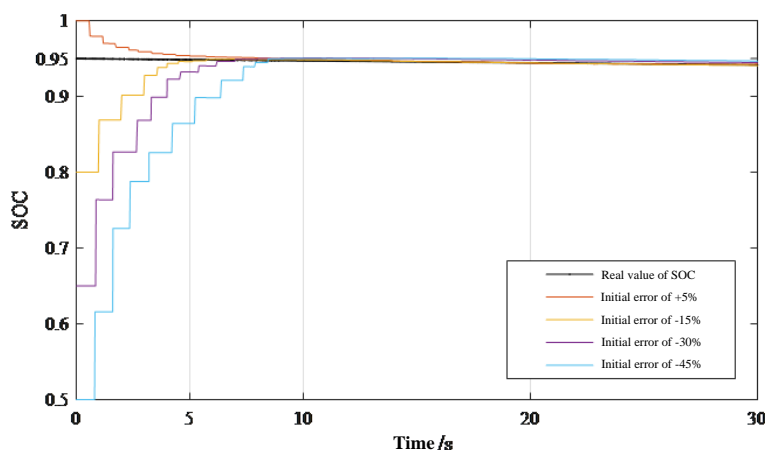
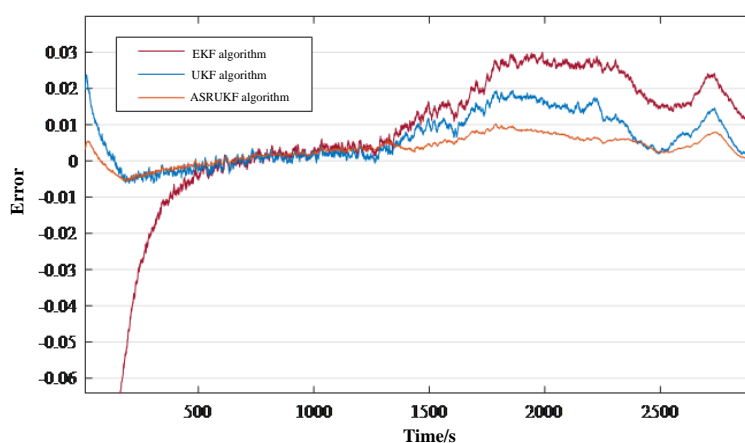


Figure 9. Convergence rate of ASRUKF algorithms under different initial values

As shown in Figure 9, the ASRUKF algorithm can converge rapidly, corresponding to different initial values. When the error is small, the algorithm can complete the correction and convergence within 5s quickly, and the process can be controlled within 10s when the error is significant.

The errors of the three algorithms in the SOC estimation process are analyzed below, as shown in Figure 10. Due to the large initial error and slow convergence speed of the EKF algorithm, the error before convergence at the beginning of the EKF algorithm is not discussed temporarily, and the maximum error after stabilization is 3.01%. The maximum error of the UKF algorithm appeared after the initial convergence, which is 2.36%. The stability error in the middle part and later could be kept within 2%, and the maximum error is 1.95%. The maximum error of ASRUKF algorithm simulation is 0.53% after the convergence of the front segment, and the stability error in the middle segment and later can be kept within 1%, and the maximum is 1.02%. Besides, the error curve of EKF and UKF algorithms fluctuates greatly, which is caused by the noise in the system. However, the curve of the ASRUKF algorithm fluctuates less, which is caused by better square root algorithm and adaptive filtering algorithm.



**Figure 10.** The contrast of estimation errors of each algorithm under 45% initial error

The simulation in the pulse discharge mode uses 1C current, a single discharge cycle of 1000s, and a pulse duty cycle of 20%. The comparison between the estimated results of the three algorithms and the true values of SOC is shown in Figure 11. In this simulation, the true value of SOC at the initial moment is selected as 100%, and the initial SOC value of the three algorithms is selected as 100%, with the initial error of 0. According to the overall situation in Figure 11, all the three algorithms can converge and fit the real SOC value, which is difficult for comparison and analysis. Then, the error curves of the three algorithms are drawn, as shown in Figure 12.

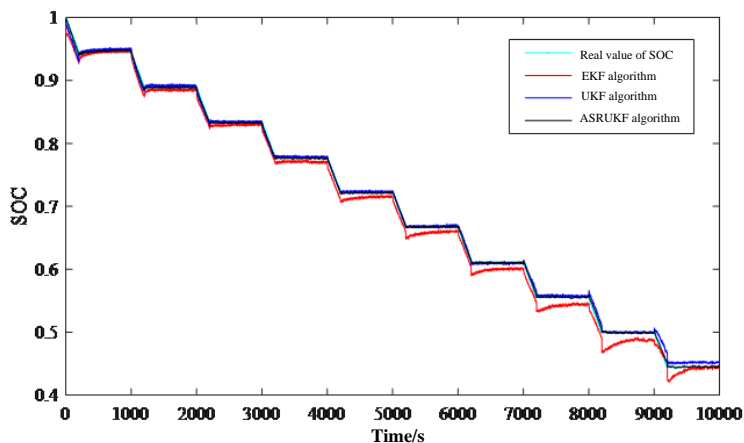


Figure 11. SOC estimation in pulse discharge mode

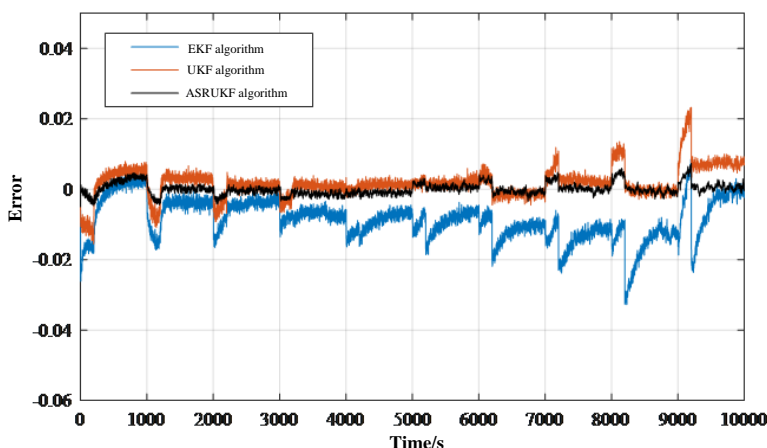
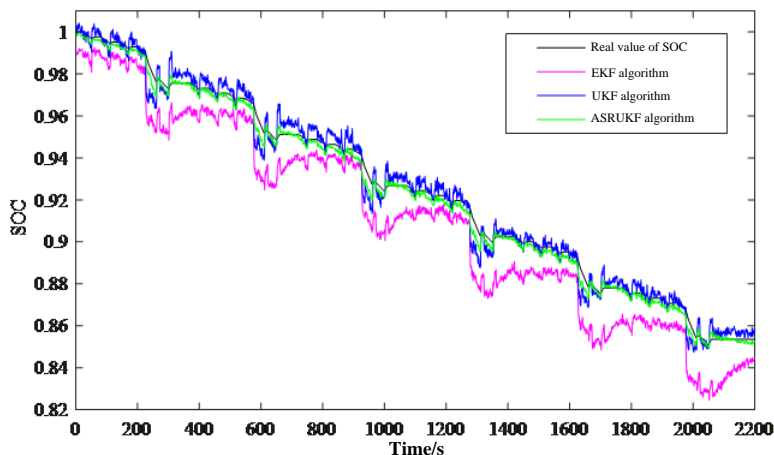


Figure 12. SOC estimation errors under the mode of pulse discharge

The maximum error of the EKF algorithm is 3.28% (Figure 12), which occurs in the pulse discharge. The maximum error of the UKF algorithm is 2.26%. The maximum error of the ASRUKF algorithm is 0.74%, and all of them occur at the time of pulse discharge. When the battery is switched from the discharge state to the static state, the error of the UKF and ASRUKF algorithms can fall back to a stable range quickly. The UKF algorithm keeps the error within 1%, and the ASRUKF algorithm can control within 0.5%. While the EKF algorithm cannot converge quickly. It will take a period of time for the error to fall back slowly and stabilize within 1.5%.

Finally, the simulation analysis of the DST working condition was carried out. DST is a standard condition suitable for the charging and discharging test of power battery. It is obtained from the federal urban driving schedule (FUDS) by splitting, cutting, simplifying, and combining. The comparison between the estimated value of each algorithm and the true value of SOC under the DST condition is shown in Figure 13. The true value of SOC at the initial moment is 100%, the initial value of SOC estimated by the program is 95%, the total number of 6 cycles is 2100s, and the simulation time is set as

2200s. It can be seen from the figure that the ASRUKF algorithm is the most closely aligned with the true value of SOC, the UKF algorithm follows, and the EKF algorithm has the worst fit. The error comparison of the algorithm is shown in Figure 14.



**Figure 13.** SOC estimation under DST operating conditions

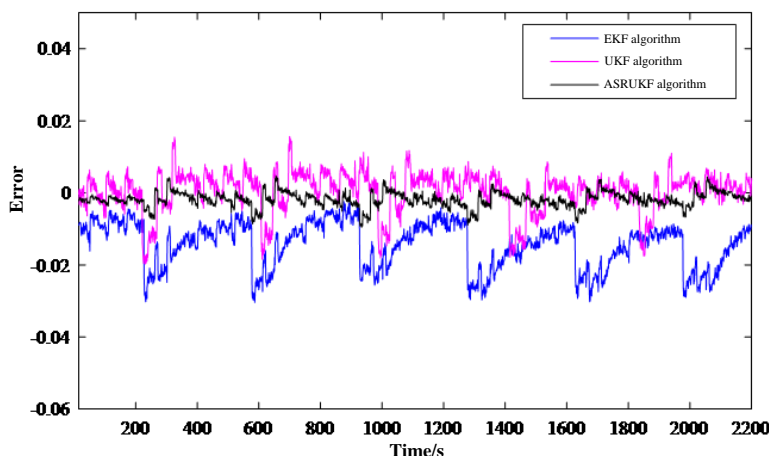


**Figure 14.** SOC estimation errors under DST operating conditions

Because the charging and discharging state and output current value of the battery change frequently under the DST condition, the fluctuation of SOC value and the error value are tremendous. The EKF algorithm has the worst estimation effect (Figure 14) and takes the longest time to correct the error, with the maximum error reaching 3.04%. The UKF algorithm is centered, with a maximum error of 1.98% and the average error of the whole segment within 1%. The ASRUKF algorithm has the best estimation effect, with the maximum error of only 0.96%, and the average error of the whole segment can be kept within 0.5%.

## 6. CONCLUSION

The research object of this paper is the single lithium-ion battery. The SOC estimation method based on 2RC-Thevenin equivalent circuit model and ASRUKF algorithm is proposed, and the corresponding simulation and experiments are carried out. The 2RC-thevenin equivalent circuit model is selected as the research model of lithium-ion battery by comparing the commonly used battery models and considering the factors of precision, complexity, and calculation. The parameters of the circuit model and the OCV-SOC curve were identified and fitted by the pulse discharge experiment, and the precision of the parameter identification was verified in the battery simulation of MATLAB/Simulink. Based on the UKF algorithm, the ASRUKF algorithm was proposed to estimate the SOC of the lithium-ion battery, and Simulink simulation analysis was carried out for the algorithm under three different conditions: constant discharge, pulse discharge, and DST. The simulation results show that the ASRUKF algorithm has better stability and faster convergence speed, and its estimation precision is better than other algorithms.

## ACKNOWLEDGMENTS

The work was supported by the Scientific Research Development Plan of Shandong Higher Education Institutions (No. J18KA316) and the Development Plan of Shandong Province (No. 2019GGX104019) and Guangdong Basic and Applied Basic Research Foundation (2019A1515110706).

## References

1. M. A. Hannan, M. S. H. Lipu and A. Hussain, *Renew. Sust. Energ. Rev.*, 78 (2017) 834-854.
2. Y. Wang, C. Zhang and Z. Chen, *Appl. Energy*, 185 (2017) 2026-2032.
3. K. Wang, L. Li and H. Zhang, *Int. J. Electrochem. Sci.*, 8 (2013) 5036-5041.
4. Z. Cabrane, M. Ouassaid and M. Maaroufi, *IET Renew. Power Gener.*, 11 (2017) 1157-1165.
5. Y. T. Zhou, Y. N. Wang, K. Wang, L. Kang, F. Peng, L. C. Wang and J. B. Pang, *Appl. Energy*, 260 (2020) 114169.
6. J. Meng, G. Luo and F. Gao, *IEEE Trans. Power Electron.*, 31 (2015) 2226-2238.
7. K. Wang, C. Li and B. Ji, *J. Mater. Eng. Perform.*, 23 (2014) 588-592.
8. X. Zhu and T. Zhang, *Electr. Eng.*, 14 (2013) 47-50.
9. K. Wang, J. B. Pang, L. W. Li, S. Z. Zhou, Y. H. Li and T. Z. Zhang, *Front. Chem. Sci. Eng.*, 12 (2018) 376-382.
10. Y. Xing, W. He and M. Pecht, *Appl. Energy*, 113 (2014) 106-115.
11. C. Xikun, S. Dong and C. Xiaohu, *Transactions of China Electrotechnical Society*, 30 (2015) 141-147.
12. G. T. Xia, Y. N. Huang, F. J. Li, L. C. Wang, J. B. Pang, L. W. Li and K. Wang, *Front. Chem. Sci. Eng.*, (2020), DOI: 10.1007/s11705-019-1901-5.
13. Y. T. Zhou, Y. N. Huang, J. B. Pang and K. Wang, *J. Power Sources*, 440 (2019) 227149.
14. X. Liu, C. Liu and Z. Yang, *Proceedings of the CSEE*, 36 (2018) 1769-1777.
15. H. H. Pan, Z. Q. Lu and J. Z. Li, *Transactions of China Electrotechnical Society*, 32 (2017) 1-8.
16. X. Feng, Y. Zhang, L. Kang, L. C. Wang, C. X. Duan, K. Yin, J. B. Pang and K. Wang, *Front. Chem.*

- Sci. Eng.*, (2020), DOI: 10.1007/s11705-020-1956-3.
17. C. Y. Bu, F. J. Li, K. Yin, J. B. Pang, L. C. Wang and K. Wang, *ACS Appl. Electron. Mater.*, 2 (2020) 863-878.
  18. K. Wang, L. W. Li, W. Xue, S. Z. Zhou, Y. Lan, H. W. Zhang and Z. Q. Sui, *Int. J. Electrochem. Sci.*, 12 (2017) 8306-8314.
  19. H. He, R. Xiong and X. Zhang, *IEEE Trans. Veh. Technol.*, 60 (2011) 1461-1469.
  20. C. Lin, H. Mu and R. Xiong, *Appl. Energy*, 166 (2016) 76-83.
  21. G. T. Xia, C. Li, K. Wang and L. W. Li, *Sci. Adv. Mater.*, 11 (2019) 1079-1086.
  22. K. Wang, L. W. Li, Y. Lan, P. Dong and G. T. Xia, *Math. Probl. Eng.*, 2019 (2019) 1-8.
  23. Y. Liu and G. J. Tan, *Transactions of China Electrotechnical Society*, 32 (2017) 108-118.
  24. C. Weng, J. Sun and H. Peng, *J. Power Sources*, 258 (2014) 228-237.
  25. Y. L. Liu, S. Dai, Z. Cheng and L. W. Zhu, *Transactions of China Electrotechnical Society*, 29 (2014) 221-228.
  26. K. Wang, S. Z. Zhou, Y. T. Zhou, J. Ren, L. W. Li and Y. Lan, *Int. J. Electrochem. Sci.*, 13 (2018) 10766-10773.
  27. D. Sun and X. K. Chen, *Proceedings of the CSEE*, 35 (2015) 185-191.
  28. D. Q. Wang, S. Zhang, M. Gan and J. L. Qiu, *IEEE Trans. Ind. Inform.*, 16 (2020) 2500-2508.
  29. X. Chen, W. Shen and M. Dai, *IEEE Trans. Veh. Technol.*, 65 (2015) 1936-1947.
  30. X. Tan, Q. Li and H. Wang, *Int. J. Electr. Power Energy Syst.*, 44 (2013) 179-191.
  31. M. Jiao, D. Q. Wang and J. L. Qiu, *J. Power Sources*, 459 (2020) 228051.
  32. M. Zhang, K. Wang and Y. Zhou, *Complexity*, 2020 (2020) 8231243.
  33. Z. W. Lian, X. Shi and X. Ke, *Power System Protection and Control*, 42 (2014) 137-142.
  34. Z. Li, P. Zhang, Z. F. Wang, Q. Song and Y. N. Rong, *Energy Procedia*, 105 (2017) 3515-3520.
  35. Q. L. Cheng, J. B. Pang, D. H. Sun, J. G. Wang, S. Zhang, F. Liu, Y. K. Chen, R. Q. Yang, N. Liang, X. H. Lu, Y. C. Ji and J. Wang, *Infomat*, 2 (2020) 656-697.
  36. F. A. Inthamoussou, J. Pegueroles-Queralt and F. D. Bianchi, *IEEE Trans. Energy Convers.*, 28 (2013) 690-697.
  37. S. Sepasi, L. R. Roose and M. M. Matsuura, *Energies*, 8 (2015) 5217-5233.
  38. X. Luo, F. L. Zhang, Q. Li, Q. T. Xia, Z. H. Li, X. K. Li, W. N. Ye, S. D. Li and C. Ge, *Journal of Physics-Condensed Matter*, 32 (2020) 334001.
  39. X. X. Wang, W. Z. Song and M. H. You, *ACS Nano*, 12 (2018) 8588-8596.
  40. M. E. Choi, S. W. Kim and S. W. Seo, *IEEE Trans. Smart Grid*, 3 (2011) 463-472.
  41. H. S. Ramadan, M. Becherif and F. Claude, *Int. J. Hydrog. Energy*, 42 (2017) 29033-29046.
  42. Q. C. Sun, X. Luo, Q. T. Xia, Y. F. Guo, J. Su, Q. Li and G. X., *J. Magn. Magn. Mater.*, 499 (2020) 166317.
  43. C. H. Li, X. J. Zhu and G. Y. Cao, *Renew. Energ.*, 34 (2009) 815-826.
  44. S. Inoue and H. Akagi, *IEEE Trans. Power Electron.*, 22 (217) 2299-2306.
  45. K. Wang, B. Ji and M. Han, *Chinese J. Inorg. Chem.*, 29 (2013) 2105-2109.
  46. D. Liu and H. Li, *IEEE Trans. Power Electron.*, 21 (2006) 1513-1517.
  47. J. Wu, K. Yin and M. Li, *Nanoscale*, 12 (2020) 4077-4084.
  48. H. L. Du, C. Y. Ma, W. X. Ma and H. T. Wang, *Process. Appl. Ceram.*, 12 (2018) 303-312.
  49. A. Muhammad and H. L. Du, *Ceram. Int.*, 46 (2019) 2238-2246.
  50. B. Hredzak, V. G. Agelidis and Jang M, *IEEE Trans. Power Electron.*, 29 (2013) 1469-1479.
  51. K. Wang, L. Zhang and B. Ji, *Energy*, 59 (2013) 440-444.
  52. K. Wang, L. Li, T. Z. Zhang and Z. F. Liu, *Energy*, 70 (2014) 612-617.
  53. R. A. Dougal, S. Liu and R. E. White, *IEEE Trans. Compon. Pack T.*, 25 (2002) 120-131.
  54. K. Wang, L. Li and H. Zhang, *Int. J. Electrochem. Sci.*, 8 (2013) 4785-4791.
  55. C. Duan, Y. Yu, J. Xiao, Y. Li, P. Yang, F. Hu and H. Xi, *Green Energy Environ.*, (2020), DOI: 10.1016/j.gee.2020.04.006.
  56. J. R. Wu, K. Yin, M. Li, Z. P. Wu, S. Xiao, H. Wang, J. A. Duan and J. He, *Nanoscale*, 12 (2020)

4077-4084.

57. Y. Li, X. Zhou, W. Qi, H. Xie, K. Yin, Y. Tong, J. He, S. Gong and Z. Li, *Chem. Eng. J.*, 383 (2020) 123086.
58. B. Xia, H. Wang and Y. Tian, *Energies*, 8 (2015) 5916-5936.
59. Z. Yu, R. Huai and L. Xiao, *Energies*, 8 (2015) 7854-7873.
60. S. F. Tang, Z. T. Wang, D. Yuan, C. Zhang, Y. D. Rao, Z. B. Wang and K. Yin, *J. Clean. Prod.*, 268 (2020) 122253.
61. Y. Han, Q. R. Zhang and L. C. Wu, *Desalination*, 477 (2020) 114270.
62. G. Lu, H. H and L. Q. Li, *ACS Nano*, 14 (2020) 6222-6231.
63. C. Duan, Y. Yu, J. Xiao, X. Zhang, L. Li, P. Yang, J. Wu and H. Xi, *Sci. China Mater.*, 63 (2020) 667.
64. X. Ying and S. Ying, *Journal of Beijing University of Aeronautics and Astronautics*, 40 (2014) 855-860.
65. K. Wang, L. Li and H. Yin, *PloS One*, 10 (2015) e0138672.
66. Y. P. Fu, J. L. Ding, H. F. Wang and J. W. Wang, *Appl. Soft Comput.*, 68 (2018) 847-855.
67. K. Sun, L. Zhang and Y. Xing, *IEEE Trans. Power Electron.*, 26 (2011) 3032-3045.
68. Y. P. Fu, M. C. Zhou, X. W. Guo and L. Qi, *IEEE Trans. Syst. Man Cybern. Syst.*, (2019) 10.1109/TSMC.2019.2907575.
69. F. Zhang, X. Teng, W. Shi, Y. Song, J. Zhang, X. Wang, H. Li, Q. Li, S. Li and H. Hu, *Appl. Surf. Sci.*, 52 (2020) DOI: 10.1016/j.apsusc.2020.146910.
70. Y. Z. Qin, Q. Li and J. Xu, *Electrochim. Acta*, 224 (2017) 90-95.
71. Y. Li, C. Wang and J. Gong, *Energy*, 109 (2016) 933-946.
72. K. Wang, L. Li and T. Zhang, *Energy*, 70 (2014) 612-617.
73. H. X. Liu, L. Zhao, Y. T. Zhou, J. Y. Song, K. Wang and L. W. Li, *Sci. Adv. Mater.*, 11 (2019) 1072-1078.
74. C. Z. Zhu, Y. Z. Ma and Q. K. Bu, *Int. J. Electrochem. Sci.*, 13 (2018) 10207-10216.
75. H. Gholizade-Narm and M. Charkhgard, *IET Power Electron.*, 6 (2013) 1833-1841.
76. M. Charkhgard and M. Farrokhi, *IEEE Trans. Ind. Electron.*, 57 (2010) 4178-4187.
77. Z. Q. Dai, K. Wang and L. W. Li, *Int. J. Electrochem. Sci.*, 8 (2013) 9384-9389.
78. Y. N. Huang, L. C. Wang and K. Wang, *Complexity*, 2019 (2019) 7824743.
79. J. R. Wu, K. Yin, M. Li, S. Xiao, Z. P. Wu, K. Wang and J. A. Duan, *Colloids Surf. A Physicochem. Eng. Asp.*, (2020) 125030.
80. S. F. Tang, Z. T. Wang, D. L. Yuan, Y. T. Zhang, J. B. Qi, Y. D. Rao, G. Lu, B. Li, K. Wang and K. Yin, *Int. J. Electrochem. Sci.*, 15 (2020) 2470-2480.
81. W. He, N. Williard and C. Chen, *Int. J. Electr. Power Energy Syst.*, 62 (2014) 783-791.
82. W. He, N. Williard and C. Chen, *Microelectron. Reliab.*, 53 (2013) 840-847.
83. L. Wang, R. Yan, F. Bai, T. K. Saha and K. Wang, *IEEE Trans. Sustain. Energy*, (2020) 1109/tste.2020.2970214.
84. D. L. Yuan, C. Zhang, S. F. Tang, M. T. Sun, Y. T. Zhang, Y. D. Rao, Z. B. Wang and J. Ke, *Sci. Total Environ.*, 727 (2020) 138773.
85. S. F. Tang, J. C. Tang, D. L. Yuan, Z. T. Wang, Y. T. Zhang and Y. D. Rao, *RSC Adv.*, 10 (2020) 17627-17634.
86. K. S. Ng, C. S. Moo and Y. P. Chen, *Appl. Energy*, 86 (2009) 1506-1511.
87. M. Mastali, J. Vazquez-Arenas and R. Fraser, *J. Power Sources*, 239 (2013) 294-307.
88. Y. P. Fu, Y. Wang, D. Wu and H. F. Wang, *Transport Res A-Pol*, 138 (2020) 172-186.
89. C. Hu, B. D. Youn and J. Chung, *Appl. Energy*, 92 (2012) 694-704.
90. Y. P. Fu, H. F. Wang, G. D. Tian, Z. W. Li and H. S. Hu, *J. Intell. Manuf.*, 30 (2019) 2257-2272.
91. F. Sun, X. Hu and Y. Zou, *Energy*, 36 (2011) 3531-3540.
92. Q. Xue, Y. H. Yang, Z. W. Gao, *Appl. Phys. Lett.*, 109 (2016) 192407.
93. Q. F. Gao, Y. Han, P. Y. Liang and J. Meng, *Phys. Chem. Chem. Phys.*, 22 (2020) 6291-6299.

94. R. Xiong, F. Sun and Z. Chen, *Appl. Energy*, 113 (2014) 463-476.

95. Y. He, X. T. Liu and C. B. Zhang, *Appl. Energy*, 101 (2013) 808-814.

© 2020 The Authors. Published by ESG ([www.electrochemsci.org](http://www.electrochemsci.org)). This article is an open access article distributed under the terms and conditions of the Creative Commons Attribution license (<http://creativecommons.org/licenses/by/4.0/>).